Mg-Ba-Sr-Nd isotopic evidence for a mélange origin of early Paleozoic arc magmatism

Lu-Lu Hao[1, 2, 3, 4*], Xiao-Yun Nan[1, 2*], Andrew C. Kerr[5], Si-Qi Li[1], Yuan-Bao Wu[6], Hao Wang[7], Fang Huang[1, 2]

[1] CAS Key Laboratory of Crust-Mantle Materials and Environments, School of Earth and Space Sciences, University of Science and Technology of China, Hefei 230026, China

[2] CAS Center for Excellence in Comparative Planetology, University of Science and Technology of China, Hefei, Anhui 230026, China

[3] State Key Laboratory of Isotope Geochemistry, Guangzhou Institute of Geochemistry, Chinese Academy of Sciences (CAS), Guangzhou 510640, China

[4] CAS Center for Excellence in Deep Earth Science, Guangzhou, 510640, China

[5] School of Earth and Environmental Sciences, Cardiff University, Cardiff, CF10 3AT, UK

[6] State Key Laboratory of Geological Processes and Mineral Resources, Center for Global Tectonics, School of Earth Sciences, China University of Geosciences, Wuhan 430074, China

[7] State Key Laboratory of Lithospheric Evolution, Institute of Geology and Geophysics, CAS, Beijing, 100029, China

*Corresponding authors:

Lu-Lu Hao (haolulu1990@126.com); Xiao-Yun Nan (nanxiaoy@ustc.edu.cn)

ABSTRACT

In recent years, the mélange model has been increasingly considered as an important way to transfer slab components to arc sources in modern subduction zones. This model differs from the classic slab fluid/melt metasomatism model in that it invokes physical mixing of bulk sediment, altered oceanic crust (AOC), serpentinite, and mantle wedge at the slab-mantle interface. However, due to the lack of subducted sediment compositions, the mélange model has not been applied to any significant extent in paleo-subduction zones. The lack of evidence for bulk AOC and serpentinite components in mélange sources also hinders our understanding of any mélange origin for arc-type magmas. Here, we report Mg-Ba-Sr-Nd isotope compositions of the early Paleozoic Fushui mafic rocks in the Qinling orogen of central China, to trace their origin and constrain slab component transfer. The Fushui mafic rocks show typical arc-type geochemical features and enriched Sr-Nd isotope compositions, indicating the likely contribution of subducted sediments. They have low Rb/Ba ratios (< 0.1), and most samples show $\delta^{138/134}$Ba values of -0.38 to +0.10‰, similar to those of sediments (-0.2 to +0.1‰) but lower than those of MORBs (+0.03 to +0.14‰), indicating that these low $\delta^{138/134}$Ba values are most likely derived from sediment components. One Fushui sample has a high $\delta^{138/134}$Ba of +0.31‰, similar to that of AOC (up to +0.4‰). This high $\delta^{138/134}$Ba is not correlated with fluid input; instead, it results from the contribution of bulk AOC. The Fushui rocks exhibit variable δ^{26}Mg values (-0.23 to -0.11‰), slightly higher than those of MORBs. This most likely reflects ^{26}Mg-enriched subducted serpentinite components in their source. Our results not only identify the variable slab components (sediment, AOC, and serpentinite) in the arc source, but also suggest that these slab components may be transferred to their arc source by the mélange process. This study therefore provides solid evidence for the generation of arc magmas by mélange processes in paleo-subduction zones, which confirms an important role for the mélange model in slab material transport.

Keywords: subduction zones; mélange model; slab component transport; Mg-Ba isotopes; arc magmas.

1. Introduction

Subduction zones are the focal points of mass transfer between the surface and the deep Earth. Variable slab components including seafloor sediment, altered oceanic basaltic crust (AOC), oceanic abyssal peridotites, and mantle wedge serpentinite at the slab-mantle interface can all be recycled into the sub-arc mantle and contribute to arc sources. Tracing specific recycled components and the physical processes of crustal material transfer from subducting slab to the overlying mantle wedge is critical for our understanding of the evolution of Earth's chemical budget, thermal structure, and arc formation in convergent margins (e.g., Rudnick, 1995; Elliott, 2004). In most conventional subduction zone models, fluids and melts are proposed to be released during slab dehydration and fusion (e.g., McCulloch and Gamble, 1991; Elliott et al., 1997). Such fractionated components from the slab can metasomatize the overlying mantle wedge, which melts partially to produce arc magmas. In these mantle metasomatism models, it is usually difficult to identify the fluid sources from the AOC or metaperidotite (e.g., Hacker, 2008; Walowski et al., 2015; Cooper et al., 2020).

Behn et al. (2011) have compiled the geochemistry of metamorphosed sedimentary rocks that have been exposed to 2.7 to 5 GPa (approximately corresponding to sub-arc depths) during subduction. They found that the sediment melt signature (e.g., enrichment of Th and Nd) in arcs cannot form unless the sedimentary rocks have experienced temperatures > 1050 °C. However, the slab surface cannot have such high temperatures at similar pressures. In light of these issues, an increasing number of studies have proposed a mélange diapir model as an important alternative way of transferring slab components and forming arc magmas (Savov et al, 2005, 2007; Marschall and Schumacher, 2012; Nielsen and Marschall, 2017; Suga and Yeh, 2020). The mélange model (Marschall and Schumacher, 2012) proposes that at fore-arc depth, the slab components (sediment, AOC, and serpentinite) physically mix with the mantle wedge peridotite just above the slab in a subduction channel to form hybrid hydrated mélange rocks. Subsequently, the low mechanical strength of the hydrous mélange rocks triggers the formation of mechanical instabilities and the formation of buoyant diapirs of mélange material. The mélange diapir rises in a diagonal path, due to the disturbance of the corner flow in the mantle wedge (Marschall and Schumacher, 2012). Finally, the mélange partially melts in the hot corner at sub-arc depth to produce arc magmas. In contrast to mantle metasomatism models that envisage the fractionated components (i.e., slab fluids and sediment melts) move directly into the arc source, the mélange model (Nielsen and Marschall, 2017) proposes that un-differentiated slab components (bulk sediment, AOC, and serpentinite) are transferred to the arc source by the mélange diapir and that trace element fractionation in arc magmas are produced by partial melting of the mélange.

The fractionated components (sediment melts and slab fluids) have much higher Sr/Nd ratios than do their respective bulk counterparts, thus, mixing curves between the mantle and these components in Sr-Nd isotope space would have different shapes. Therefore, Nielsen and Marschall (2017) suggested that a Sr-Nd isotope plot could be a very effective means of discriminating between the two models. They showed that lavas from some modern arcs (e.g., Marianas) closely follow the mixing lines between the mantle and bulk sediment rather than sediment melts/slab fluids. In addition, some arc magmas with low Sr isotope ratios and Nd/Sr values plot within a 'forbidden AOC fluid/sediment melt zone' (Nielsen and Marschall, 2017). Moreover, the melting experiments of the mélange rocks have yielded melts that have typical arc-like trace-element patterns (Cruz-Uribe et al., 2018; Codillo et al., 2018). All these observations indicate that the mélange model could be an important mechanism to transfer the slab components and to generate arc magmas in modern arcs.

However, the mélange model has not been applied to any significant extent in paleo-subduction zones. This is principally because the detailed compositions of subducted sediments cannot be easily constrained in paleo-subduction zones. This therefore makes it difficult to assess the importance of the mélange model through the geological record. Furthermore, in addition to sediments, the mélange contains significant components of subducted AOC and serpentinite (Marschall and Schumacher, 2012; Codillo et al., 2018), which also have important implications for the generation of arc magmas. For example, the AOC component is inferred to play a key role in providing sufficient accessory minerals (e.g., rutile, zircon, and REE-bearing minerals of the perovskite supergroup) that control the distinctive trace element patterns observed in subduction-related magmas (Cruz-Uribe et al., 2018). However, the contributions of bulk AOC and serpentinite in arc magmas remain debated (e.g., Tomanikova et al, 2019), thus hindering our understanding of the mélange origin for subduction-related magmas.

Oceanic abyssal peridotites have high δ^{26}Mg [$\delta^{26}Mg = [(^{26}Mg/^{24}Mg)_{sample} / (^{26}Mg/^{24}Mg)_{DSM3} - 1] \times 1000$ (‰)] values (up to +0.03‰) due to seafloor weathering (Liu et al., 2017). The mantle wedge serpentinites (e.g., talc-rich serpentinites) at the slab-mantle interface also show high δ^{26}Mg (Li et al., 2018). These metaperidotites have much higher MgO contents than subducted sediment and AOC. Therefore, Mg isotope compositions of arc magmas can be used to trace serpentinite components in their source because the distinctive δ^{26}Mg values at high MgO are easily recognizable. Recent studies have also suggested that Ba isotope compositions of arc magmas have the potential to trace AOC components (Nielsen et al., 2020; Wu et al., 2020). This is because: (1) serpentinites typically have very low Ba concentrations (Savov et al., 2005, 2007), since the mantle rock protoliths are Ba-poor and the serpentinization processes do not add significant Ba; instead, the Ba budget of arc magmas is mainly derived from AOC and sediment; (2) compared to low $\delta^{138/134}$Ba [$\delta^{138/134}Ba = [(^{138/134}Ba_{sample})/(^{138/134}Ba_{SRM3104a}) - 1] \times 1000$ (‰)] values (-0.2 to +0.1‰) of sediments, AOC can have high $\delta^{138/134}$Ba (up to +0.4‰) (Nielsen et al., 2018). In this study, we report Ba-Mg-Sr-Nd isotope compositions of early Paleozoic arc-type mafic rocks in the Qinling orogen of central China, to trace specific slab components in their arc source and constrain the possible transport mechanism of material from the slab.

2. Geological setting and samples

The Qinling orogen in central China is divided into the South and North Qinling orogens by the Shangdan suture (Fig. 1a) (Wang et al., 2014). Three fault-bounded, penetratively deformed units constitute the North Qinling orogen, from north to south, which are the Kuanping, Erlangping and North Qinling units (Fig. 1a). The North Qinling unit between the southern Shangdan fault and northern Zhuyangguan-Xiaguan fault represents the oldest basement rocks in the North Qinling belt, and includes mainly gneisses, amphibolites, marble, and eclogites (Zheng et al., 2020). The Fushui intrusive complex in the North Qinling unit is intruded into biotite gneiss (Fig. 1b) and mainly consists of monzodiorites with minor hornblende gabbros. Zircon U-Pb dating shows that these mafic rocks formed at ~488 to 484 Ma (Wang et al., 2014), i.e., early Paleozoic. The major and trace element data of our studied Fushui mafic rocks are available in Wang et al. (2014). These rocks have variable SiO_2 and MgO contents ranging from 46.4 to 55.3 wt.% and 3.4 to 9.2 wt.% (volatile-free), respectively. They display arc-like trace-element characteristics with enrichments in light rare earth elements (LREEs), large ion lithophile elements (LILEs), Pb, and depletion in high field strength elements (HFSEs) and heavy REEs (HREEs) (Wang et al., 2014). They were previously considered to be derived from a mantle source metasomatized by Shangdan (Paleo-Tethys) ocean subduction beneath the North Qinling unit (Wang et al., 2014; Zheng et al., 2020). However, the specific slab components in their arc source remain unclear. In this study, we revisit the Fushui mafic rocks and report new Mg-Ba-Sr-Nd isotopic compositions.

3. Analytical methods

Mineral element analyses and back-scattered electron imaging were carried out at State Key Laboratory of Isotope Geochemistry, Guangzhou Institute of Geochemistry (GIG), Chinese Academy of Sciences (CAS), by using a JXA-8100 electron microprobe. A 15 kV accelerating voltage, 20 nA beam current, and 2 μm beam diameter were employed. The analytical procedures were described in detail in Huang et al. (2007). The 1σ precision was < ± 3%.

Whole-rock Sr-Nd isotopic analyses were performed in the CAS Key Laboratory of Crust-Mantle and Environments at the University of Science and Technology of China (USTC), Hefei. The chemical purification procedures were described in detail by Chen et al. (2007). Approximately 120 to 150 mg of sample powder was digested in a mixture of concentrated HF–HNO_3-HCl. Strontium and light rare earth elements were isolated on quartz columns by conventional-ion exchange chromatography (Chen et al., 2007) with a

2 ml resin bed of AG 50 W-X8 cation exchange resin (200 to 400 mesh). Neodymium and Sm were separated from other rare earth elements on quartz columns using 1.7 ml Teflon powder coated with HDEHP, di(2-ethylhexyl) orthophosphoric acid, as the cation exchange medium. The total procedural blanks were < 0.5 ng for Sr and < 0.05 ng for Nd. The Sr-Nd isotopic measurements were conducted on a Neptune Plus multi-collector inductively coupled plasma mass spectrometer (MC-ICP-MS). The mass bias produced by the instrument were normalized by $^{86}Sr/^{88}Sr$ = 0.1194 and $^{146}Nd/^{144}Nd$ = 0.7219, respectively. The $^{87}Sr/^{86}Sr$ of the reference materials NBS-987 and BHVO-2 are 0.710249 ± 0.000012 (2SD, n=28) and 0.703469 ± 0.000019 (2SD, n=3), respectively. The $^{143}Nd/^{144}Nd$ ratios of the reference materials JNdi-1 and BHVO-2 are 0.512124 ± 0.000018 (2SD, n=24) and 0.512991 ± 0.000009 (2SD, n=3), respectively. Our results of the standard materials are consistent with Weis et al. (2006).

The Mg and Ba isotopes were also analyzed at USTC. The detailed descriptions of sample dissolution, chemical purification and mass spectrometry analysis can be found in An et al. (2014) for Mg isotopic analyses and Nan et al. (2015) for Ba isotopic analyses. Briefly, sample powders were digested using double-distilled HF-HNO_3-HCl before column chemistry. Then, sample solutions with ~10 mg Mg were uploaded to columns containing 2 ml Bio-Rad AG50W-X12 cation exchange resin (200 to 400 mesh). The purification procedure was performed twice to effectively separate Mg from matrix elements. For Ba, sample solutions with ~2 μg Ba were uploaded to the 2 ml (first column) and 0.5 ml (second column) AG50-X12 resin. The yields of Mg and Ba during purification procedures were > 99%. The total procedural blank for Mg was < 10 ng and for Ba was < 2 ng. The Mg and Ba isotopic analyses were carried out on the same MC-ICP-MS. Magnesium isotope ratios were measured by sample-standard bracketing in a low-resolution mode. The results are reported in standard δ notation relative to the international reference material DSM-3: $\delta^{x}Mg = [(^{x}Mg/^{24}Mg)_{sample} / (^{x}Mg/^{24}Mg)_{DSM3} - 1] \times 1000$ (‰), where X = 25 or 26 and DSM-3 is an international reference solution standard made from pure Mg metal (Galy et al., 2003). The external precision of $\delta^{26}Mg$ based on the long-term measurements of two in-house reference solutions (CAM-1 and IGG) is better than 0.05‰ (2SD). The measured $\delta^{26}Mg$ values of USGS standards (-0.15 ± 0.02‰ for BCR-2, -0.17 ± 0.03‰ for BHVO-2, and -0.16 ± 0.03‰ for AGV-1) agree well with previously published values (An et al., 2014). Barium isotope ratios were measured by the double-spike method in a low-resolution mode under "dry" plasma conditions. The results are reported in δ-notation relative to the international reference material NIST SRM3104a (Horner et al., 2015; Nan et al., 2015): $\delta^{137/134}Ba = [(^{137/134}Ba_{sample})/(^{137/134}Ba_{SRM3104a}) - 1] \times 1000$ (‰). For direct comparison with recent Ba isotope data in the literature, $\delta^{138/134}Ba$ values of all samples are calculated following the mass-dependent fractionation laws ($\delta^{138/134}Ba \approx 1.33 \times \delta^{137/134}Ba$; Young et al., 2002) and displayed in the Appendix. The external precision of $\delta^{137/134}Ba$ based on the long-term measurements of the two in-house standards (USTC-Ba and ICPUS-Ba) is better than 0.04‰ (2SD). We estimate the long-term external precision of $\delta^{138/134}Ba$ is better than 0.05‰ (2SD), which has been verified by Deng et al. (2021). The $\delta^{137/134}Ba$ values yielded in this study (Table S1) for the two USGS reference materials, i.e., 0.05 ± 0.02‰ for BCR-2 and 0.05 ± 0.02‰ for AGV-1, are in good agreement with previously published values (Nan et al., 2015).

4. Results

The whole-rock Sr-Nd-Mg-Ba isotope data and mineral composition data of the Fushui mafic rocks are given in the Appendix.

4.1 Rock classification and mineral compositions

The Fushui mafic rocks are massive and show fine-grain to coarse-grain textures. Their distinct mineral assemblages suggest that they can be divided into two types of rocks: hornblende gabbros and monzodiorites (Figs. S1-S2). The hornblende gabbros mainly consist of hornblende (40 to 45 vol.%) and plagioclase (35 to 45%) with minor biotite (3 to 10%), clinopyroxene (0 to 5%), and quartz (0 to 5%). Rare olivine grains are only present in some samples, and are subhedral and partly altered to iddingsite or talc (Zheng et al., 2020). Accessory minerals of titanite, apatite, zircon, and Fe-Ti oxides are occasionally observed. The monzodiorites mainly comprise plagioclase (40 to 50%), K-feldspar (15 to 30%), biotite (5 to 15%), hornblende (0 to 15%), clinopyroxene (0 to 10%), and quartz (0 to 5%) along with accessory titanite, apatite, zircon, and Fe-Ti oxides. Generally, compared to the hornblende gabbros, the monzodiorites comprise more K-feldspar and less hornblende.

The plagioclase grains in the hornblende gabbros exhibit SiO_2, Al_2O_3, Na_2O, and CaO contents (in wt.%) of 53.6 to 58.6, 25.5 to 26.3, 5.0 to 7.0, and 8.2 to 12.7, respectively, with the mole fraction of anorthite of 39 to 58, and so are andesine and labradorite. The hornblende in the hornblende gabbros shows variable FeO (12.5 to 20.9 wt.%) and MgO (7.7 to 13.1 wt.%), high CaO (11.1 to 12.8 wt.%), and low Na_2O (1.0 to 1.8 wt.%) contents. The biotite, with high K_2O (9.2 wt.%) and BaO (0.71 to 0.75 wt.%) contents, is the primary K- and Ba-bearing mineral in the hornblende gabbros. The plagioclase in the monzodiorites has variable SiO_2, Al_2O_3, Na_2O, and CaO contents (in wt.%) of 54.8 to 66.4, 21.3 to 28.3, 5.3 to 6.8, and 5.7 to 11.0, respectively, with the mole fraction of anorthite of 32-52. The K-feldspar in the monzodiorites is characterized by high SiO_2 (63.7 to 64.2 wt.%), Al_2O_3 (18.4 to 20.1 wt.%), K_2O (12.9 to 14.2 wt.%), and BaO (0.9 to 1.6 wt.%) contents and is mainly orthoclase with the mole fraction of orthoclase of 75 to 92. The hornblende and biotite in the monzodiorites show similar element compositions (e.g., high K_2O and BaO contents in the biotite) to those in the hornblende gabbros. The clinopyroxene in the monzodiorites has low Mg# values of 66 to 78 and high CaO contents of 18.9 to 21.5 wt.% and is diopside and augite.

4.2 Alteration effects

Mineral chemistry can be used to evaluate the degree of alteration of a rock. If the magmatic rocks have been significantly affected by alteration, the main mineral phases will not retain their original igneous signatures and chemical compositions. The petrographic (Fig. S1) and back-scattered electron images (Fig. S2) of the Fushui mafic rocks reveal the well-preserved primary minerals (e.g., hornblende, K-feldspar, clinopyroxene, and biotite), and limited epidotization in some plagioclase grains and iddingsitization and talc alteration in the rare olivine grains (Zheng et al., 2020). This is consistent with their low loss on ignition (LOI) values (0.1 to 1.9 wt.%) (Wang et al., 2014). The primary minerals also retain their original chemical compositions as shown above. Thus, the Fushui mafic rocks appear to have undergone insignificant post-magmatic alteration. Indeed, the major elements (e.g., Si, Mg, Fe, Al, Ca, Na, K) show no systematic correlations with increasing LOI in both the Fushui monzodiorites and hornblende gabbros (except for sample 10QL111) (Fig. S3). Sample 10QL111 with the highest LOI contents (1.9 wt.%) has the lowest Na and Fe but highest Ca contents among the hornblende gabbros, likely reflecting the alteration of these elements to some extent during the plagioclase epidotization.

The majority of LILEs can be variably mobilized whereas HFSEs, REEs and Th are relatively immobile during a range of weathering, hydrothermal, and low-grade metamorphic processes (e.g., Pearce, 2014). However, the Fushui mafic rocks show subparallel coherent REE and trace-element patterns (Wang et al., 2014), suggesting that these elements were relatively immobile during post-magmatic alteration. For example, Sr and Pb of the Fushui monzodiorites and hornblende gabbros show no obvious correlations with increasing LOI (Figs. S4a-b). The immobility of Rb and Ba is consistent with the very fresh K-feldspar and biotite grains in the Fushui mafic rocks.

The Mg-Ba-Sr-Nd isotopic compositions of the Fushui monzodiorites and hornblende gabbros do not correlate with LOI values (Figs. S4c-f), consistent with the immobility of these elements as discussed above. Thus, they represent the original isotopic signatures of the Fushui mafic rocks.

4.3 Whole-rock compositions

A general problem in interpreting mafic plutonic rocks relates to whether they represent true liquid compositions or, alternatively, are cumulates (e.g., Jagoutz et al., 2011). The Fushui hornblende gabbros (except for sample 10QL111) have SiO_2 (46.4 to 49.8 wt.%), total-alkali (3.8 to 6.5 wt.%) and MgO (5.2 to 9.2 wt.%) contents, and Mg# (42 to 64) values (Fig. 2). These major element compositions overlap with those of the Cuijiu non-cumulate hornblende gabbros from the early Mesozoic Gangdese arc crust, but are different from those of the Cuijiu cumulate hornblende gabbros (Xu et al., 2019) (Fig. 2). Furthermore, the Fushui hornblende gabbros have similar mineral proportions (e.g., hornblende, plagioclase) and petrological texture to the Cuijiu non-cumulate hornblende gabbros (see Fig. 4f in Xu et al., 2019), whereby the hornblende and plagioclase occur as euhedral to mostly subhedral grains (Figs. S1a-b, 2e). Coarse-grained and subhedral quartz grains can be occasionally observed (Figs. S1b, 2e). Conversely, the Cuijiu cumulate hornblende gabbros show typical orthocumulate textures with cumulus hornblende and interstitial plagioclase (Xu et al., 2019), which are not observed in the Fushui hornblende gabbros. Thus, we suggest that the Fushui hornblende gabbros were crystallized from basaltic liquid with limited crystal accumulation, indicating that they approach the liquid compositions. Compared to the Fushui hornblende gabbros, the monzodiorites have higher SiO_2 (52.9 to 55.3 wt.%) and total-alkali (6.9 to 7.8 wt.%) but lower MgO (3.4 to 4.5 wt.%) contents (Fig. 2). They belong to the alkaline magma series. Generally, the Fushui mafic rocks show similar major element compositions (e.g., Si, K, Mg, Al, Ca) to experimental melts of mélange rocks (Fig. 2). For example, Cruz-Uribe et al. (2018) reported that mélange materials were partially melted at upper mantle conditions to produce alkaline magmas with intermediate compositions (SiO_2 = 51 to 61 wt.%) (Fig. 2). More mantle peridotites and less sediments involved in the mélange source could decrease K_2O and SiO_2 contents of experimental melts to produce tholeiitic to calc-alkaline magmas (Fig. 2) (Codillo et al., 2018).

The Fushui mafic rocks display typical arc-type trace-element patterns with enrichments in LREEs, LILEs (e.g., Rb, Ba), Th, and Pb, and depletions in HFSEs (e.g., Nb, Ta) and HREEs (see Wang et al., 2014 for details). The Fushui hornblende gabbros have similar patterns but lower Th contents relative to the monzodiorites. Accordingly, the former has lower Th/Nd ratios than the latter.

The Fushui mafic rocks show higher Sr isotope ratios ($^{87}Sr/^{86}Sr(i)$ = 0.7098 to 0.7151) and lower Nd isotope ratios ($\varepsilon_{Nd}(t)$ = -5.79 to -4.10) than the primitive mantle, i.e., enriched Sr-Nd isotope compositions (Fig. 3a). The Fushui monzodiorites have slightly more enriched Sr-Nd isotopes than the hornblende gabbros. These two types of rocks show identical $\delta^{26}Mg$ values with a variable range of -0.23 to -0.11‰, similar to those of the Lesser Antilles arc lavas (-0.25 to -0.10‰, Teng et al., 2016), which extend to be higher than those of MORBs (-0.25 ± 0.06‰, 2SD) and mantle peridotites (-0.25 ± 0.04‰, 2SD) (Teng et al., 2010) (Figs. 4a, c-d). The Fushui mafic rocks have highly heterogeneous Ba isotope compositions with $\delta^{138/134}Ba$ = -0.38 to +0.31‰, much wider than the range of unaltered MORBs (+0.03 to +0.14‰; Nielsen et al., 2018, 2020) (Figs. 5a-b). Except for sample 11QL84 which has much higher $\delta^{138/134}Ba$ (+0.31‰), the Fushui hornblende gabbros show similar $\delta^{138/134}Ba$ values (-0.38‰ to +0.10‰) to the monzodiorites ($\delta^{138/134}Ba$ = -0.33 to 0.00‰) (Fig. 5). There are no obvious correlations between $\delta^{138/134}Ba$ values and Ba/Th ratios in both the Fushui hornblende gabbros and monzodiorites (Fig. 5d).

5. Discussion

5.1 Mantle melting, crustal assimilation and fractional crystallization

Although the Fushui monzodiorites and hornblende gabbros show very similar REE and trace-element patterns and Sr-Nd isotopic compositions, the monzodiorites cannot be produced by fractional crystallization from the gabbroic magmas. The Fushui mafic complex is dominated by the monzodiorites with minor hornblende gabbros. This is inconsistent with fractional crystallization which generally requires a corresponding abundance of gabbroic rocks (e.g., Jagoutz et al., 2011). Furthermore, if fractional crystallization occurred during the generation of the Fushui monzodiorites, the hornblende should be the primary fractionated mineral as indicated by the differences of the mineral assemblages between the hornblende gabbros and monzodiorites (Figs. S1-2). However, the two types of rocks have similar Dy/Yb ratios (Fig. 4b), which is inconsistent with hornblende fractionation, as this should form a clearly negative trend on the SiO_2 vs. Dy/Yb plot. Thus, combined with the mineralogy, and low SiO_2, and high MgO and Mg# of the Fushui monzodiorites, we suggest that they were derived from partial melting of a hydrated ultramafic mantle lithology. Given their similar trace-element patterns and Sr-Nd isotopic compositions, the Fushui monzodiorites and hornblende gabbros were most likely formed by partial melting of a common mantle source.

The Fushui mafic rocks are characterized by crust-like geochemical features such as arc-type REE and trace-element patterns and very enriched Sr-Nd isotope compositions (Fig. 3a). The possibility exists that these chemical fingerprints reflect crustal assimilation with wall-rock during emplacement or mantle source metasomatism. The assimilation and fractional crystallization model (Wang et al., 2014) considering the Shangdan oceanic arc basalt and the North Qingling gneiss as the original mantle-derived magma and the contaminant, respectively, has shown that a high rate of assimilation ($R > 0.7$) is required to produce the Sr-Nd isotope signatures of the Fushui mafic rocks, which is unreasonable (Taylor, 1980). This model would also result in obvious differences in the HREE contents between the modeled melt and the Fushui mafic rocks (Wang et al., 2014). Furthermore, if mafic magmas were contaminated by the continental crust during their ascent, they would show synchronous changes in major-trace element and radiogenic and stable (e.g., Sr, Nd, Ba, Mg) isotope compositions. Although the Fushui mafic rocks exhibit somewhat variable whole-rock $^{87}Sr/^{86}Sr(i)$ ratios of 0.7098 to 0.7151, they have relatively constant whole-rock εNd(t) values of -5.79 to -4.10. In addition, both the Fushui monzodiorites and hornblende gabbros have whole-rock Sr-Nd-Ba-Mg isotope compositions that are not correlated with SiO_2 contents (Figs. 4c, 5a, S5a-b). Their $^{87}Sr/^{86}Sr(i)$ and $\delta^{138/134}Ba$ values are also not correlated with Sr and Ba contents, respectively (Figs. S5c-d). Their $\delta^{26}Mg$ values are also not negatively correlated with their CaO contents (Fig. S5e). This indicates no marked assimilation of marbles, given the marbles generally show very low $\delta^{26}Mg$ values (e.g., S-J. Wang et al., 2014). All of these features indicate negligible crustal contamination. Thus, the crustal geochemical fingerprint of these rocks is related to their metasomatized mantle source.

Previous studies suggested that both the Fushui monzodiorites and hornblende gabbros have experienced olivine and clinopyroxene but no plagioclase, K-feldspar, or hornblende fractional crystallization during ascent of the primitive magmas (Wang et al., 2014; Zheng et al., 2020). However, fractional crystallization of these minerals cannot cause detectable Mg isotope fractionation (Teng et al., 2016). Garnet may crystallize from basaltic melts at high pressures (Macpherson et al., 2006). Garnet has much lower $\delta^{26}Mg$ than coexisting clinopyroxene and olivine, so garnet removal would result in residual melts with elevated ^{26}Mg and high La/Yb ratios. However, the high $\delta^{26}Mg$ values of the Fushui mafic rocks cannot be attributed to garnet fractionation from a basaltic magma, because the $\delta^{26}Mg$ values of both the monzodiorites and hornblende gabbros remain nearly constant with increasing La/Yb ratios (Fig. 4a). Overall, therefore, the lack of correlation between $\delta^{26}Mg$ and SiO_2 or MgO (Figs. 4c-d) suggests that the high $\delta^{26}Mg$ values of the Fushui mafic rocks are not produced by magma evolution but inherited from a mantle source containing ^{26}Mg-enriched subducted components. Likewise, the $\delta^{138/134}Ba$ values of the Fushui mafic rocks do not correlate with SiO_2 contents (Fig. 5a), suggesting that fractional crystallization has not significantly modified their Ba isotope compositions. This is consistent with the high incompatibility of Ba during basaltic magma differentiation (Nielsen et al., 2020) and that no K-feldspar or biotite fractionation occurred during the formation of the Fushui mafic rocks. Thus, the variable Ba isotope ratios of the Fushui mafic rocks are also inherited from their mantle source.

Collectively, the geochemical compositions of the Fushui mafic rocks are not significantly affected by post-magmatic alteration or crustal contamination, which means that their arc-type trace-element patterns, enriched Sr-Nd isotope compositions, high $\delta^{26}Mg$ values and variable Ba isotopic ratios are primarily inherited from their mantle sources.

5.2 Slab components in the mantle source

The arc-like trace-element patterns, along with very high $^{87}Sr/^{86}Sr(i)$ ratios and negative εNd(t) values (Fig. 3a) (Wang et al., 2014; Zheng et al., 2020) of the Fushui mafic igneous rocks suggest significant involvement of slab components (e.g., AOC and sediment) in their mantle source. Such very enriched Sr-Nd isotope compositions are also observed in some modern arc alkaline magmatic rocks (see Fig. DR1 in Cruz-Uribe et al., 2018). Slab subduction is the most effective tectonic mechanism for transporting crustal materials into the mantle. Given that the AOC and serpentinite remain depleted in Nd isotopes during alteration (e.g., White et al., 2014), the very low εNd(t) values and high Th/Nd ratios of the Fushui mafic rocks (Fig. 3b) clearly indicate a subducted terrigenous sediment component in their mantle source. Notably, the Fushui monzodiorites have higher SiO_2, K_2O, Th contents, and Rb/Sr ratios than the hornblende gabbros. The monzodiorites also have slightly more enriched Sr-Nd isotope compositions than the hornblende gabbros (Figs. 3c-e). This can further verify the contribution of subducted sediments to the enriched Sr-Nd isotope compositions.

The high Ba/Th (Fig. 3f) and high Ba/La ratios in the Fushui mafic rocks generally indicate the contribution of an AOC component. Furthermore, some syn-magmatic zircon grains from the Fushui mafic rocks have low $\delta^{18}O$ values (down to 2.0‰) (Zheng et al., 2020). These low $\delta^{18}O$ values cannot be ascribed to the contribution of the fluids in the local crust because these low-$\delta^{18}O$ zircons have slightly more depleted Hf isotope compositions than the high-$\delta^{18}O$ zircons. Instead, the low $\delta^{18}O$ signatures are likely derived from a mantle source containing oceanic basaltic crust, which has experienced high-temperature hydrothermal alteration (Zheng et al., 2020).

Serpentinite components may occur in the source of the Fushui mafic rocks but cannot be easily identified. For example, fluids derived from dehydrated serpentinites can equilibrate with AOC or can induce sediment melting before entering the mantle wedge. Furthermore, we cannot effectively determine the specific forms of slab components. For example, in the classic mantle metasomatism model, the fractionation of some key trace element ratios (e.g., Ba/Th, Ba/La, Th/Nd and Th/La) can be ascribed to slab dehydration or sediment melting due to the different melt-/fluid-mobilities of these elements. In the mélange model, although physical mixing of bulk slab components cannot fractionate these elements, partial melting of the mélange can produce magmas with fractionated trace element ratios (Cruz-Uribe et al., 2018; Codillo et al., 2018).

5.2.1 Ba isotope compositions trace the AOC component

Rb/Ba ratios have been used to investigate the source of Ba in arcs (Nielsen et al., 2020). Rb and Ba are not significantly fractionated during partial melting of the upper mantle, and the most recent compilation of MORB data yielded a mean Rb/Ba ratio of 0.092 ± 0.004 (Gale et al., 2013). Most subducted sediments have average Rb/Ba < 0.1 whereas AOC is always characterized by Rb/Ba > 0.35 due to significant Rb precipitation from seawater during hydrothermal alteration. Moreover, slab fluids/melts and mélange melts all show little Rb/Ba fractionation compared to the bulk starting composition. Therefore, it is clear from Fig. 5b that Ba in the Fushui mafic rocks is mainly derived from sediments. Thus, the low $\delta^{138/134}$Ba values (-0.38 to +0.10‰) exhibited by most Fushui samples are most likely caused by sediment input to the source, since sediments usually have relatively low $\delta^{138/134}$Ba values of -0.2 to +0.1‰ (e.g., Nielsen et al., 2020). Furthermore, Nielsen et al. (2018, 2020) and Wu et al. (2020) have also clearly demonstrated that sediment addition into the mantle could produce low $\delta^{138/134}$Ba values. Barium isotope fractionation can further occur during both sediment melting and mélange melting, which can help explain the much lower $\delta^{138/134}$Ba values (up to -0.38‰) of the Fushui mafic rocks.

Although the low Rb/Ba of the Fushui mafic rocks clearly indicates a sediment contribution, the possibility that their arc source contains significant AOC components cannot be precluded. Given the very high Ba concentrations in subducted sediments, even if there is substantially more AOC material with minor sediment in the slab, the Ba budget of arcs can still be dominated by sediments, resulting in arc rocks with low Rb/Ba. This scenario was observed in the Aleutian arc (Nielsen et al., 2020), which contains significant AOC components but still has low Rb/Ba. Modelling by Nielsen et al. (2020) showed that the low Rb/Ba ratios of the Aleutian arc (< 0.08) can still be produced even with a high mass ratio (7-16) between bulk AOC and bulk sediment or with a high mass ratio (~3) between AOC fluids and sediment melts. Notably, although almost all the Aleutian arc samples have $\delta^{138/134}$Ba values lower than or equal to subducting sediments, there is still one sample showing a higher $\delta^{138/134}$Ba value than these sediments. This high-$\delta^{138/134}$Ba component is likely to have originated from AOC (Nielsen et al., 2020). We likewise suggest that the high-$\delta^{138/134}$Ba (+0.31‰) sample 11QL84 could also indicate a contribution from AOC (e.g., AOC-fluids or bulk AOC) in their source. Indeed, of all the potential components only AOC exhibits the very high $\delta^{138/134}$Ba values (up to +0.4‰) (Nielsen et al., 2018, 2020).

5.2.2 Serpentinite component revealed by Mg isotope compositions

The AOC fluids and sediment melts in subduction zones typically show much lower Mg contents than mantle peridotites, and cannot significantly modify Mg isotope compositions of the mantle. The classic subduction model also includes fluid flux from dehydrating serpentinite in the lithospheric mantle of the subducting plate (Cooper et al., 2020). Given that the subducted oceanic abyssal peridotites generally display high δ^{26}Mg values (up to +0.03‰) due to seafloor alteration (Liu et al., 2017), Teng et al. (2016) suggested that the high δ^{26}Mg of the Lesser Antilles arc lavas could be caused by the addition of Mg-rich fluids from subducted oceanic abyssal peridotites. However, we contend that the high δ^{26}Mg values of arc magmas are not induced by such Mg-rich fluids for two reasons: (1) substantial fluids are introduced into the sub-arc mantle by the breakdown of antigorite in subducted oceanic peridotites. The δ^{26}Mg of antigorite is not significantly different from olivine (Beinlich et al., 2014). Moreover, Wang et al. (2019) showed that aqueous Mg^{2+} is enriched in lighter Mg isotope compositions compared to serpentine. (2) Most importantly, boron isotopes of sub-arc mantle xenoliths from the Avachinsky volcano of the Kamchatka clearly show fluid metasomatism by AOC and serpentinite (Tomanikova et al., 2019), yet the mantle xenoliths from the same area still display mantle-like δ^{26}Mg values (-0.30 to -0.21‰, Hu et al., 2020) (Fig. 4d). This indicates that the fluids released from AOC and serpentinite could not significantly introduce high $\delta^{26}Mg$ into the sub-arc mantle.

Bulk AOC and sediment do not significantly contribute to the high $\delta^{26}Mg$ of arc magmas. For example, in the Lesser Antilles arc, a large proportion of sediments (> 50%) is required to produce high $\delta^{26}Mg$ due to the much lower Mg contents in sediment compared with peridotite (Teng et al., 2016) (Fig. 4d). This would yield much more enriched Sr-Nd isotope compositions than those observed in the Lesser Antilles arc. Furthermore, if high $\delta^{26}Mg$ values are dominated by sediments, samples with higher $^{87}Sr/^{86}Sr$ and lower $^{143}Nd/^{144}Nd$ should have higher $\delta^{26}Mg$. However, the $\delta^{26}Mg$ values of the Lesser Antilles arc remain nearly constant with variable Sr-Nd isotope ratios (Figs. 4e-f). Additionally, a mantle source involving a high proportion of sediments is unlikely to produce low-Si and high-Mg rocks (Teng et al., 2016).

In this study, the Fushui mafic rocks show relatively homogeneous Sr-Nd isotope signatures, indicating that sediment contributions did not change significantly (Fig. 3a). Thus, their variable and high $\delta^{26}Mg$ cannot be caused by bulk sediment contributions. This is confirmed by the flux-weighted $\delta^{26}Mg$ (-0.34‰) of Global Subducting Sediments (Hu et al., 2017) which is lower than that of the average mantle (-0.25 ± 0.04‰, 2SD, Teng et al., 2010). Although AOC has variable $\delta^{26}Mg$ (e.g., -1.70 to +0.21‰ for the AOC from the Ocean Drilling Program Hole 801C in the Pigafetta Basin, Huang et al., 2018) and generally higher average $\delta^{26}Mg$ (0.00 ± 0.09‰, Huang et al., 2018) than the mantle, this cannot fully explain the high $\delta^{26}Mg$ values. A simple mixing model shows that adding 30%-90% AOC to the mantle wedge can produce $\delta^{26}Mg$ that ranges from -0.23 to -0.11‰ (Fig. 4d). However, a mantle source with large amounts of AOC cannot generate basaltic melts; instead, it produces andesitic to trondhjemitic melts (Castro et al., 2010).

Conversely, as shown above, oceanic abyssal peridotites generally show high $\delta^{26}Mg$ due to seafloor alteration (Liu et al., 2017). Additionally, meta-peridotites (e.g., talc-rich serpentinite) at the slab-mantle interface also show high $\delta^{26}Mg$ values (up to -0.01‰) (Beinlich et al., 2014; Li et al., 2018). Such meta-peridotites, as a bulk component, can contribute to high $\delta^{26}Mg$ values of arc magmas.

5.3 A mélange origin for Fushui mafic rocks

In the preceding discussion a range of subducted components (sediment, AOC, serpentinite) have been identified in the source of the Fushui mafic rocks. However, the specific transport mechanism for these components remains unclear. Here, we propose that they are most likely transported into the arc source as individual bulk components (i.e., by the mélange model).

As shown above, low and high $\delta^{138/134}Ba$ values of the Fushui mafic rocks are derived from subducted sediments and AOC, respectively. Notably, Ba is highly fluid-mobile, and Ba/Th ratios of arc magmas can be largely influenced by AOC-released fluids. If AOC-fluids contribute to the high $\delta^{138/134}Ba$ values, a positive correlation between Ba/Th and $\delta^{138/134}Ba$ should be expected in the high-Ba/Th samples, similar to that seen in the Tonga arc (Wu et al., 2020). However, such a correlation is absent in the Fushui hornblende gabbros (Fig. 5d): the high-$\delta^{138/134}Ba$ sample does not have the highest Ba/Th ratio. Thus, the high $\delta^{138/134}Ba$ of the Fushui rocks is most likely to be derived from bulk AOC. Conversely, the low $\delta^{138/134}Ba$ values in the Fushui rocks could be ascribed to contributions of bulk sediment. If $\delta^{138/134}Ba$ values (-0.2 to +0.1‰) of subducted sediments (Nielsen et al., 2020) are used, mixing between bulk sediment and depleted mantle can explain the Ba isotope compositions of most Fushui samples (Fig. 5c). Two samples show slightly lower $\delta^{138/134}Ba$ values, which could be caused by partial melting of the mélange rocks (Nielsen et al., 2020). Additionally, high $\delta^{26}Mg$ values of the Fushui mafic rocks indicate the contribution of subducted bulk serpentinite, as discussed above. Furthermore, on a Sr-Nd isotope plot (Fig. 3a), the Fushui mafic rocks are close to the mixing line between the depleted mantle and bulk sediment, rather than its melts. Finally, the Fushui mafic rocks show major-element compositions very similar to the experimental melts of the mélange rocks (Fig. 2) (Cruz-Uribe et al., 2018; Codillo et al., 2018).

Therefore, based on the evidence presented above, we propose a mélange model for generation of the Fushui arc-type mafic rocks. The sediment, AOC, serpentinite, and mantle wedge firstly mix mechanically at the slab-mantle interface to form the mélange rocks. Then partial melting of the mélange diapir could produce Fushui arc-type mafic rocks, whose Sr-Nd and Mg isotope compositions are dominated by subducted sediment and serpentinite, respectively, in the mélange source. Their low and high $\delta^{138/134}$Ba values reflect the contributions of bulk sediment and AOC, respectively.

5.4 Implications for recycling of slab components

In conventional subduction models slab components are widely considered to be transferred into sub-arc mantle source in the forms of fluids and melts in a subduction zone (e.g., Elliott et al., 1997). An increasing number of studies have suggested that the mélange diapir model could be an effective way to transport slab components to arc source (e.g., Marschall and Schumacher, 2012; Nielsen and Marschall, 2017; Cruz-Uribe et al., 2018; Codillo et al., 2018). The mélange model emphasizes the bulk slab components (bulk sediment, AOC, and serpentinite) being transported into the arc source (Nielsen and Marschall, 2017). The mélange origin for arc magmas is well constrained by the Sr-Nd isotope compositions of mafic lavas in modern arcs, which can effectively trace the bulk sediment component (rather than sediment melts) in the arc source.

While the mélange model has been widely applied in modern subduction zones, it has not been significantly proposed for paleo-subduction zones due to the lack of compositions of subducted sediments. This study indicates that high δ^{26}Mg and $\delta^{138/134}$Ba values of arc-type magmas may effectively trace the subducted bulk serpentinite and AOC, respectively, and so our results are particularly useful in verifying the mélange model in paleo-subduction zones. Thus, our data from a paleo-arc combined with the Cenozoic cases from modern arcs, lend further support to the mélange processes being a significant mechanism for transporting slab material and generating arc magmas.

6. Summary

(1) The early Paleozoic Fushui mafic rocks in the Qinling orogen of central China show arc-type geochemical characteristics and enriched Sr-Nd isotope compositions.

(2) The Fushui mafic rocks show δ^{26}Mg values of -0.23 to -0.11‰, which extend to be higher those of MORBs. This most likely reflects ^{26}Mg-enriched subducted serpentinite components in their arc source.

(3) Most samples of the Fushui rocks show $\delta^{138/134}$Ba values of -0.38 to +0.10‰, similar to those of sediments but lower than those of MORBs, indicating the contribution of sediment components. One Fushui sample has a high $\delta^{138/134}$Ba of +0.31‰, which may be derived from bulk AOC (altered oceanic basaltic crust).

(4) Our results not only identify the variable slab components (sediment, AOC and serpentinite) in the arc source, but also suggest that these slab components may be transferred to their arc source by the mélange process. This study therefore provides solid evidence for the generation of arc magmas by mélange processes in paleo-subduction zones.

Acknowledgements

We thank Editor Rosemary Hickey-Vargas, Ivan Savov, Jason Harvey, and Ping-Ping Liu for their insightful and critical reviews that greatly improved the manuscript. We also thank W-Y Li, H-M Yu, J Xu, L-L Tian, and Z Zeng for their assistance with isotopic analysis. This work is supported by the Strategic Priority Research Program (B) of Chinese Academy of Sciences (Grant No. XDB18000000) and the National Science Foundation of China (42073007, 41721002, 41873005, 41802048).

References

An, Y.J., Wu, F., Xiang, Y., Nan, X.Y., Yu, X., Yang, J., 2014. High-precision Mg isotope analyses of low-Mg rocks by MC-ICP-MS. Chem. Geol., 390, 9-21.

Behn, M.D., Kelemen, P.B., Hirth, G., Hacker, B.R., Massonne, H.-J., 2011. Diapirs as the source of the sediment signature in arc lavas. Nat. Geosci., 4, 9, 641-646.

Beinlich, A., Mavromatis, V., Austrheim, H., Oelkers, E.H., 2014. Inter-mineral Mg isotope fractionation during hydrothermal ultramafic rock alteration-Implications for the global Mg-cycle. Earth Planet. Sci. Lett., 392, 166-176.

Castro, A., Gerya, T., García-Casco, A., Fernández, C., Díaz Alvarado, J., Moreno-Ventas, I., Loew, I., 2010. Melting relations of MORB-sediment mélanges in underplated mantle wedge plumes: Implications for the origin of cordilleran-type batholiths. J. Petrol., 51, 1267-1295.

Chen, F., Li, X.H., Wang, X.L., Li, Q.L., Siebel, W., 2007. Zircon age and Nd-Hf isotopic composition of the Yunnan Tethyan belt, southwestern China. Int. J. Earth. Sci., 96, 1179-1194.

Codillo, E., Le Roux, V., Marschall, H., 2018. Arc-like magmas generated by mélange-peridotite interaction in the mantle wedge. Nat. Commun, 9, 1, 1-11.

Cooper, G.F., Macpherson, C.G., Blundy, J.D., Maunder, B., Allen, R., Goes, S., Collier, J., Bie, L., Harmon, N., Hicks, S., Iveson, A., Prytulak, J., Rietbrock, A., Rychert, C., Davidson, J., the VoiLA team, 2020. Variable water input controls evolution of the Lesser Antilles volcanic arc. Nature, 582, 525-529.

Cruz-Uribe, A.M., Marschall, H.R., Gaetani, G.A., Le Roux, V., 2018. Generation of alkaline magmas in subduction zones by partial melting of mélange diapirs-An experimental study. Geology, 46, 4, 343-346.
Deng, G., Kang, J., Nan, X., Li, Y., Guo, J., Ding, X., Huang, F., 2021. Barium isotope evidence for crystal-melt separation in granitic magma reservoirs. Geochim. Cosmochim. Acta., 292, 115-129.
Elliott, T., 2004. Tracers of the Slab: in Inside the Subduction Factory 1st edn vol. 138 (ed. Eiler, J.) 23-45 (Geophys. Monogr. Ser., Am. Geophys. Union).
Elliott, T., Plank, T., Zindler, A., White, W., Bourdon, B., 1997. Element transport from slab to volcanic front at the Mariana arc. J. Geophys. Res. Solid Earth, 102, 14991-15019.
Gale, A., Dalton, C.A., Langmuir, C.H., Su, Y.J., Schilling, J.G., 2013. The mean composition of ocean ridge basalts. Geochem. Geophys. Geosyst., 14, 489-518.
Galy, A., Yoffe, O., Janney, P.E., Williams, R.W., Cloquet, C., Alard, O., 2003. Magnesium isotope heterogeneity of the isotopic standard SRM980 and new reference materials for magnesium-isotope-ratio measurements. J. Anal. At. Spectrom., 18 (11), 1352-1356.
Hacker, B.R., 2008. H_2O subduction beyond arcs. Geochem. Geophys. Geosyst., 9(3): Q03001.
Horner, T.J., Kinsley, C.W., Nielsen, S.G., 2015. Barium isotopic fractionation in seawater mediated by barite cycling and oceanic circulation. Earth Planet. Sci. Lett., 430, 511-522.
Hu, Y., Teng, F.-Z., Ionov, D.A., 2020. Magnesium isotopic composition of metasomatized upper sub-arc mantle and its implications to Mg cycling in subduction zones. Geochim. Cosmochim. Acta, 278, 219-234.
Hu, Y., Teng, F.-Z., Plank, T., Huang, K.-J., 2017. Magnesium isotopic composition of subducting marine sediments. Chem. Geol., 466, 15-31.
Huang, K.-J., Teng, F.-Z., Plank, T., Staudigel, H., Hu, Y., Bao, Z.-Y., 2018. Magnesium isotopic composition of altered oceanic crust and the global Mg cycle. Geochim. Cosmochim. Acta, 238, 357-373.
Huang, X.L., Xu, Y.G., Lo, C.H., Wang, R.C., Lin, C.Y., 2007. Exsolution lamellae in a clinopyroxene megacryst aggregate from Cenozoic basalt, Leizhou Peninsula, South China: petrography and chemical evolution. Contrib. Mineral. Petrol., 154, 691-705.
Jagoutz, O., Müntener, O., Schmidt, M., Burg, J-P., 2011. The roles of flux- and decompression melting and their respective fractionation lines for continental crust formation: Evidence from the Kohistan arc. Earth Planet. Sci. Lett., 303, 1-2, 25-36.
Li, W.-Y., Teng, F.-Z., Xiao, Y., 2018. Magnesium isotope record of fluid metasomatism along the slab-mantle interface in subduction zones. Geochim. Cosmochim. Acta, 237, 312-319.
Liu, P.-P., Teng, F.-Z., Dick, H. J., Zhou, M.-F., Chung, S.-L., 2017. Magnesium isotopic composition of the oceanic mantle and oceanic Mg cycling. Geochim. Cosmochim. Acta, 206, 151-165.
Macpherson, C.G., Dreher, S. T., Thirlwall, M. F., 2006. Adakites without slab melting: high pressure differentiation of island arc magma, Mindanao, the Philippines. Earth Planet. Sci. Lett., 243, 581-593.
Marschall, H.R., Schumacher, J.C., 2012. Arc magmas sourced from mélange diapirs in subduction zones. Nat. Geosci., 5, 12, 862-867.
McCulloch, M.T., Gamble, J., 1991. Geochemical and geodynamical constraints on subduction zone magmatism. Earth Planet. Sci. Lett., 102, 3-4, 358-374.
Nan, X., Wu, F., Zhang, Z., Hou, Z., Huang, F., Yu, H., 2015. High-precision barium isotope measurements by MC-ICP-MS. J. Anal. Atom. Spectrom. 30, 2307-2315.
Nielsen, S.G., Marschall, H.R., 2017. Geochemical evidence for mélange melting in global arcs. Sci. Adv., 3, 4, e1602402.
Nielsen, S.G., Horner, T.J., Pryer, H.V., Blusztajn, J., Shu, Y., Kurz, M.D., Le Roux, V., 2018. Barium isotope evidence for pervasive sediment recycling in the upper mantle. Sci. Adv., 4, 7, eaas8675.
Nielsen, S.G., Shu, Y., Auro, M., Yogodzinski, G., Shinjo, R., Plank, T., Kay, S.M., Horner, T.J., 2020.

Barium isotope systematics of subduction zones. Geochim. Cosmochim. Acta., 275, 1-18.

Pearce, J.A., 2014. Immobile element fingerprinting of ophiolites. Elements, 10, 2, 101-108.

Plank, T., Langmuir, C.H., 1998. The chemical composition of subducting sediment and its consequences for the crust and mantle. Chem. Geol., 145, 325-394.

Rudnick, R.L., 1995. Making continental crust. Nature, 378, 571-577.

Rudnick, R.L., Gao, S., 2014. Composition of the continental crust: Treatise on Geochemistry, 4, 1-51.

Savov, I.P., Ryan, J.G., D'Antonio, M., Fryer, P., 2007. Shallow slab fluid release across and along the Mariana arc-basin system: Insights from geochemistry of serpentinized peridotites from the Mariana Fore arc. J. Geophys. Res., 112, B09205.

Savov, I.P., Ryan, J.G., D'Antonio, M., Kelley, K., Mattie, P., 2005. Geochemistry of serpentinized peridotites from the Mariana Forearc Conical Seamount, ODP Leg 125: Implications for the elemental recycling at subduction zones. Geochem. Geophys. Geosyst., 6, 4, Q04J15.

Suga, K., Yeh, M-W., 2020. Secular variation of Early Cretaceous granitoids in Kyushu, SW Japan: the role of mélange rocks as a possible magma source. Front. Earth Sci. 8, 95.

Taylor, H.P., 1980. The effects of assimilation of country rocks bymagmas on $^{18}O/^{16}O$ and $^{87}Sr/^{86}Sr$ systematics inigneous rocks. Earth Planet. Sci. Lett. 47, 243-254.

Teng, F.-Z., Hu, Y., Chauvel, C., 2016. Magnesium isotope geochemistry in arc volcanism. P. Natl. Acad. Sci., 113, 26, 7082-7087.

Teng, F.-Z., Li, W.-Y., Ke, S., Marty, B., Dauphas, N., Huang, S., Wu, F.-Y., Pourmand, A., 2010. Magnesium isotopic composition of the Earth and chondrites. Geochim. Cosmochim. Acta., 74, 14, 4150-4166.

Tomanikova, L., Savov, I.P., Harvey, J., de Hoog, J.C., Churikova, T.G., Gordeychik, B., Yogodzinski, G.M., 2019. A limited role for metasomatized subarc mantle in the generation of boron isotope signatures of arc volcanic rocks. Geology, 47, 6, 517-521.

Walowski, K., Wallace, P., Hauri, E., Wada, I., Clynne, M., 2015. Slab melting beneath the Cascade Arc driven by dehydration of altered oceanic peridotite. Nat. Geosci., 8, 404-408.

Wang, H., Wu, Y.-B., Li, C.-R., Zhao, T.-Y., Qin, Z.-W., Zhu, L.-Q., Gao, S., Zheng, J.-P., Liu, X.-M., Zhou, L., 2014. Recycling of sediment into the mantle source of K-rich mafic rocks: Sr-Nd-Hf-O isotopic evidence from the Fushui complex in the Qinling orogen. Contrib. Mineral. Petrol., 168, 4, 1062.

Wang, S-J., Teng, F-Z., Li, S-G., 2014. Tracing carbonate-silicate interaction during subduction using magnesium and oxygen isotopes. Nat. Commun, 5, 5328.

Wang, W., Zhou, C., Liu, Y., Wu, Z., Huang, F., 2019. Equilibrium Mg isotope fractionation among aqueous Mg2+, carbonates, brucite and lizardite: Insights from first-principles molecular dynamics simulations. Geochim. Cosmochim. Acta., 250, 117-129.

Weis, D., Kieffer, B., Maerschalk, C., Barling, J., De Jong, J., Williams, G.A., Hanano, D., Pretorius, W., Mattielli, N., Scoates, J.S., Goolaerts, A., Friedman, R.M., Brian Mahoney, J., 2006. High-precision isotopic characterization of USGS reference materials by TIMS and MC-ICP-MS. Geochem. Geophys. Geosyst., 7(8).

White, W.M., Klein, E.M., Holland, H.D., Turekian, K.K., 2014. Composition of the oceanic crust: Treatise on Geochemistry, 4, 457-496.

Wu, F., Turner, S., Schaefer, B.F., 2020. Mélange versus fluid and melt enrichment of subarc mantle: A novel test using barium isotopes in the Tonga-Kermadec arc. Geology, 48 (11): 1053-1057.

Xu, W., Zhu, D-C., Wang, Q., Weinberg, R., Wang, R., Li, S-M., Zhang, L-L., Zhao, Z-D., 2019. Constructing the Early Mesozoic Gangdese Crust in Southern Tibet by Hornblende dominated Magmatic Differentiation. J. Petrol., 60, 3, 515-552.

Young, E.D., Galy, A., Nagahara, H. 2002. Kinetic and equilibrium mass-dependent isotope fractionation laws in nature and their geochemical and cosmochemical significance. Geochim. Cosmochim. Acta., 66(6), 1095-1104.

Zheng, F., Dai, L.-Q., Zhao, Z.-F., Zheng, Y.-F., Ma, L.-T., Fang, W., 2020. Syn-exhumation magmatism during continental collision: Geochemical evidence from the early Paleozoic Fushui mafic rocks in the Qinling orogen, Central China. Lithos, 352, 105318.

Figure Captions

Fig. 1 (a) Geological map of the North Qinling belt with inserted map showing the Qinling orogen in central China, and (b) Simplified geological map of the Fushui intrusive rocks, showing the sampling locations, after Wang et al. (2014).

Fig. 2 Major element plots for the Fushui mafic rocks. The Fushui data are from Wang et al. (2014). The data of Gangdese arc hornblende gabbros are from Xu et al. (2019).

Fig. 3 (a) Sr-Nd isotope plot for the Fushui mafic rocks. The mixing calculations between the depleted mantle and bulk sediment, 1%, and 20% partial sediment melts follow the method of Nielsen and Marschall (2017). The depleted mantle is from Nielsen and Marschall (2017). The data of inferred local subducted sediment are from Wang et al. (2014) and Zheng et al. (2020) and are shown in Table S2. (b) εNd(t) versus Th/Nd. The data of global MORB are from White et al. (2014). (c-e) εNd(t) versus K_2O, SiO_2, and Rb/Sr, respectively. (f) Th/Nd versus Ba/Th. The data of GLOSS (global subducting sediment) and terrigenous sediment (based on the upper continental crust) are from Plank and Langmuir (1998), and Rudnick and Gao (2014), respectively.

Fig. 4 Mg isotope plots for the Fushui mafic rocks. (a) δ^{26}Mg vs. La/Yb; (b) Dy/Yb vs. SiO_2; (c) δ^{26}Mg vs. SiO_2; (d) δ^{26}Mg vs. MgO; (e) δ^{26}Mg vs. ^{87}Sr/^{86}Sr(i); (f) δ^{26}Mg vs. εNd(t). The lesser Antilles arc sediments and magmas are from Teng et al. (2016).

Fig. 5 Ba isotope plots for the Fushui mafic rocks. (a) $\delta^{138/134}$Ba vs. SiO_2; (b) $\delta^{138/134}$Ba vs. Rb/Ba; (c) εNd(t) vs. $\delta^{138/134}$Ba; (d) $\delta^{138/134}$Ba vs. Ba/Th. The Ba isotope data and Rb/Ba ratios of the MORB, AOC, depleted mantle, and sediments are from Nielsen et al. (2020). The εNd(t) values for depleted mantle and sediment are the same as Fig. 3a.

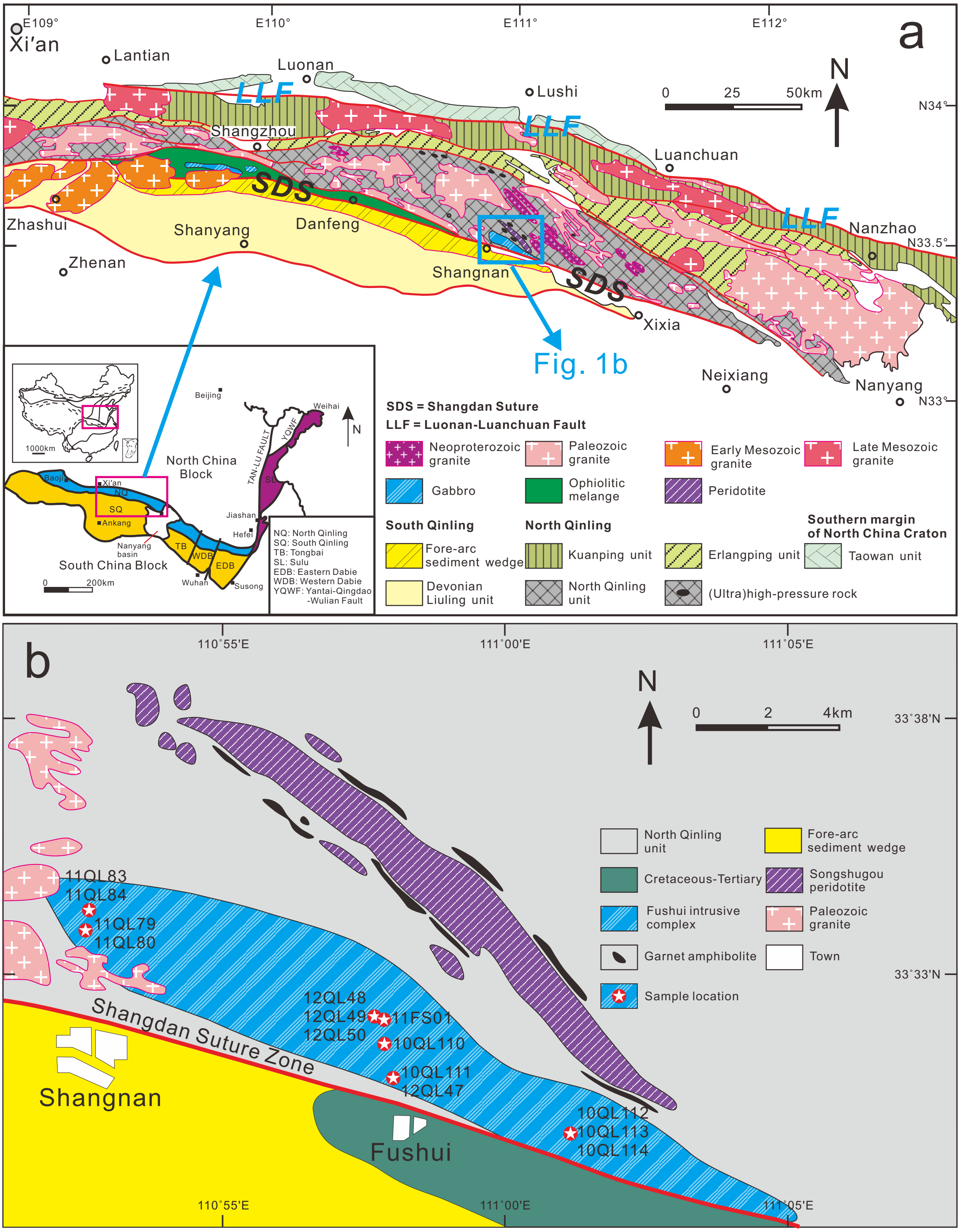
a
E109°
E110°
E111°
E112°
N34°
N33.5°
N33°
Xi'an
Lantian
Luonan
Lushi
Luanchuan
Nanzhao
Shangzhou
Zhashui
Shanyang
Danfeng
Zhenan
Shangnan
Xixia
Neixiang
Nanyang
LLF
SDS
0 25 50km
N
Fig. 1b
SDS = Shangdan Suture
LLF = Luonan-Luanchuan Fault
Neoproterozoic granite
Paleozoic granite
Early Mesozoic granite
Late Mesozoic granite
Gabbro
Ophiolitic melange
Peridotite
South Qinling
North Qinling
Southern margin of North China Craton
Fore-arc sediment wedge
Kuanping unit
Erlangping unit
Taowan unit
Devonian Liuling unit
North Qinling unit
(Ultra)high-pressure rock
1000km
Beijing
Weihai
North China Block
TAN-LU FAULT
YQWF
SL
Baoji
Xi'an
NQ
SQ
Ankang
Jiashan
Hefei
Nanyang basin
TB
WDB
EDB
South China Block
Wuhan
Susong
0 200km
NQ: North Qinling
SQ: South Qinling
TB: Tongbai
SL: Sulu
EDB: Eastern Dabie
WDB: Western Dabie
YQWF: Yantai-Qingdao -Wulian Fault
b
110°55'E
111°00'E
111°05'E
33°38'N
33°33'N
N
0 2 4km
North Qinling unit
Fore-arc sediment wedge
Cretaceous-Tertiary
Songshugou peridotite
Fushui intrusive complex
Paleozoic granite
Garnet amphibolite
Town
Sample location
11QL83
11QL84
11QL79
11QL80
12QL48
12QL49
12QL50
11FS01
10QL110
10QL111
12QL47
10QL112
10QL113
10QL114
Shangdan Suture Zone
Shangnan
Fushui

Figure

Click here to access/download;Figure;Fig. 2.pdf

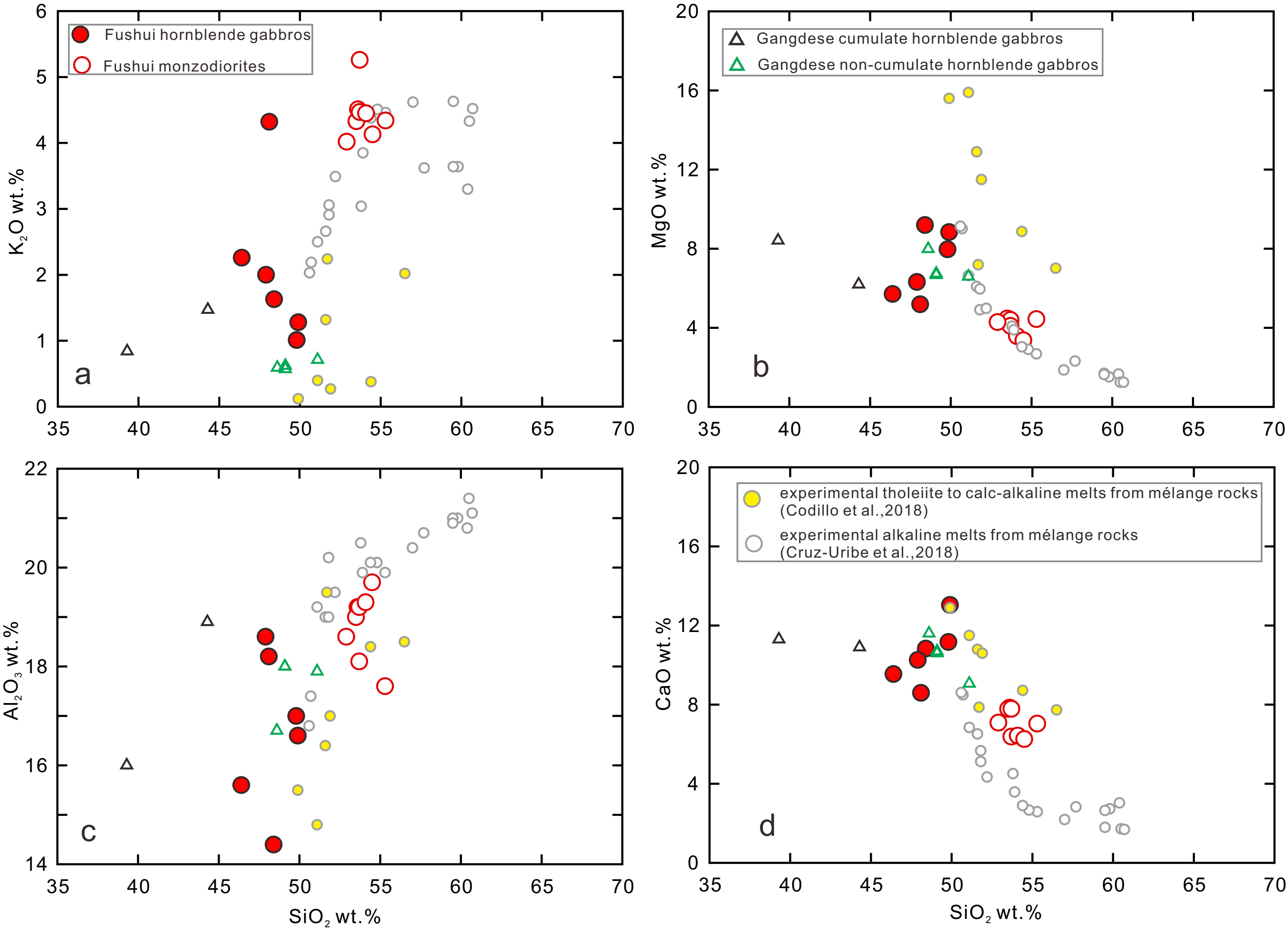

Figure

Click here to access/download;Figure;Fig. 3.pdf

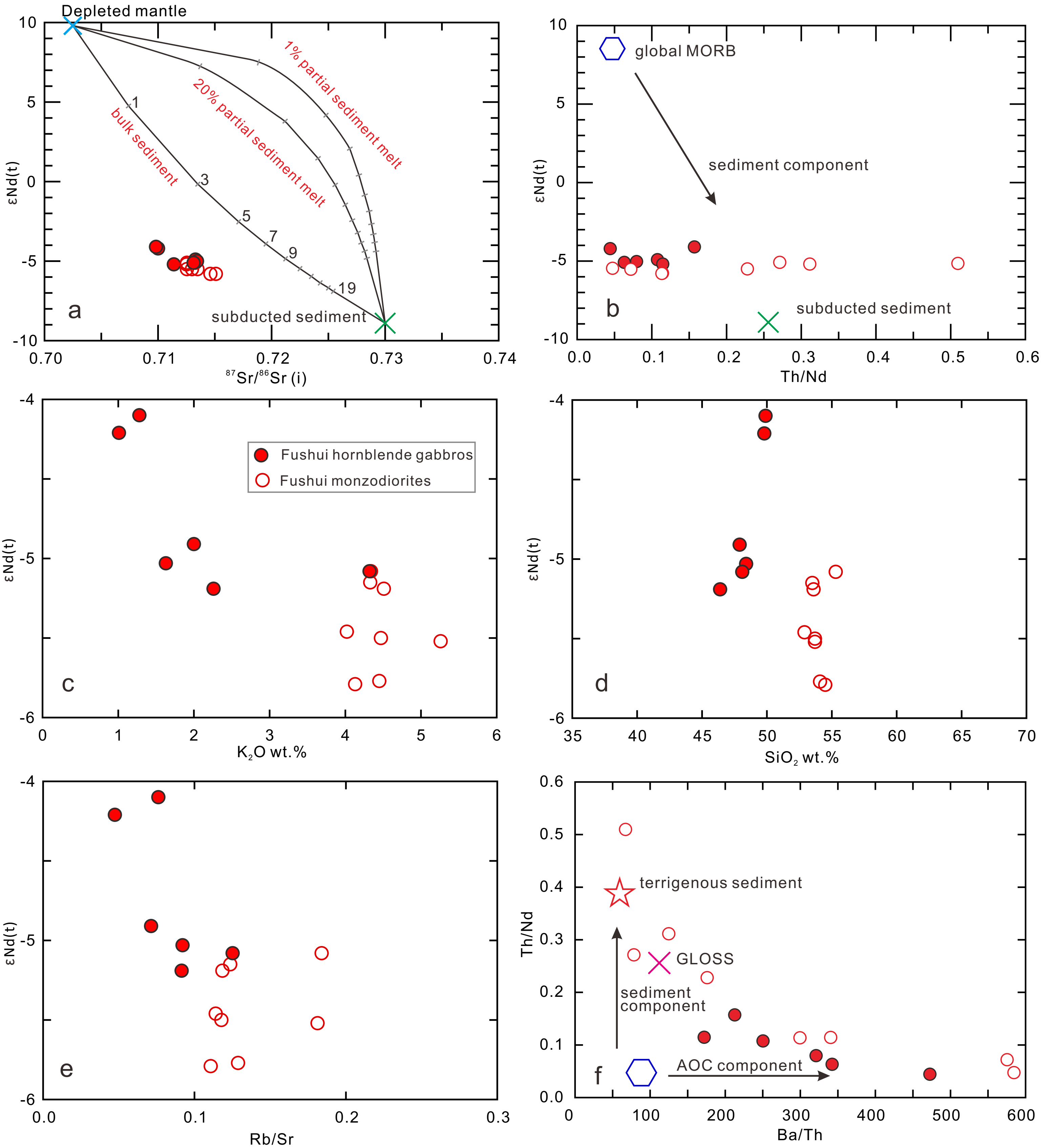

Figure

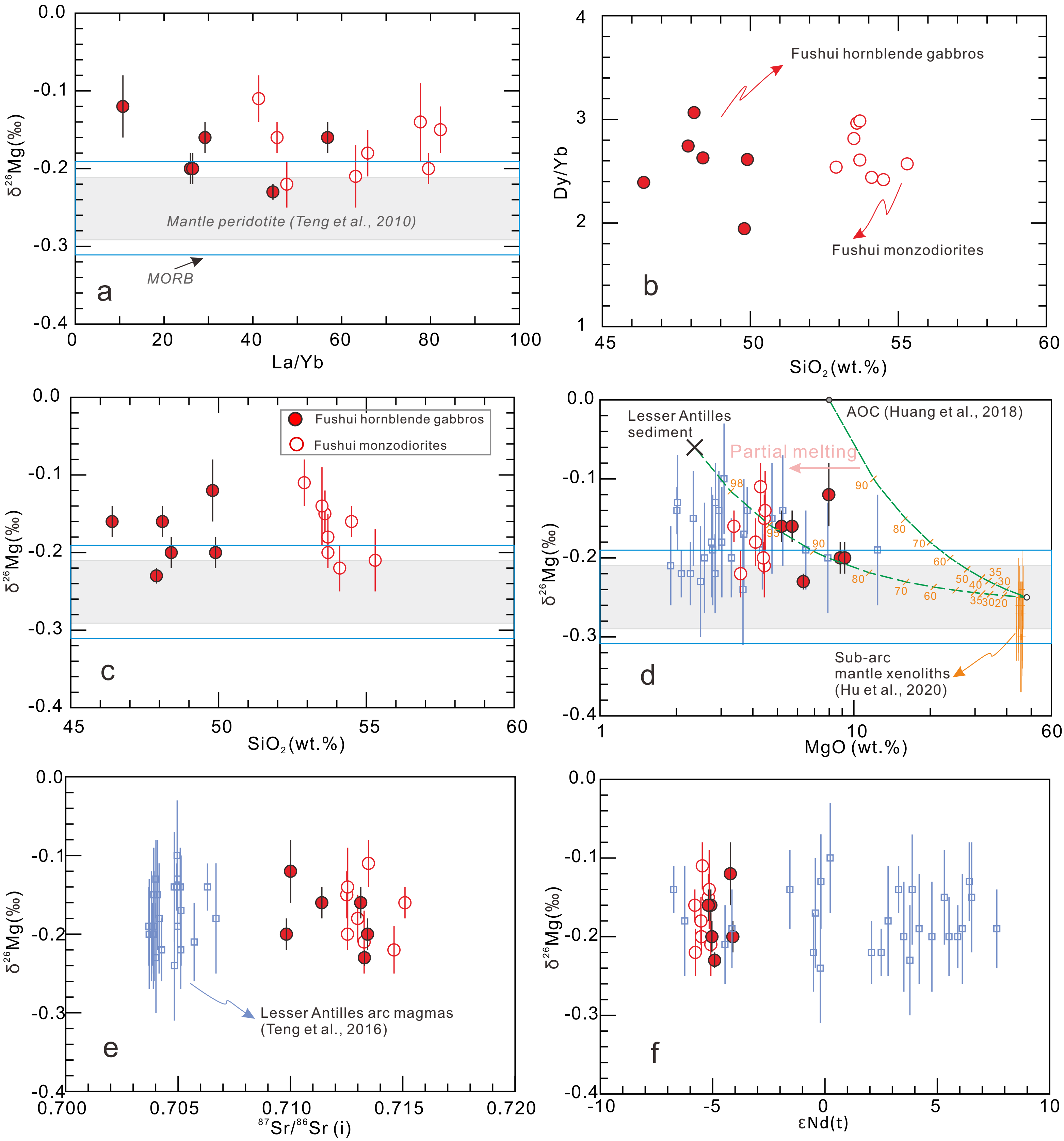

a
La/Yb
δ26Mg(‰)
Mantle peridotite (Teng et al., 2010)
MORB
b
SiO2 (wt.%)
Dy/Yb
Fushui hornblende gabbros
Fushui monzodiorites
c
SiO2 (wt.%)
Fushui hornblende gabbros
Fushui monzodiorites
d
MgO (wt.%)
Lesser Antilles sediment
AOC (Huang et al., 2018)
Partial melting
Sub-arc mantle xenoliths (Hu et al., 2020)
e
87Sr/86Sr (i)
Lesser Antilles arc magmas (Teng et al., 2016)
f
εNd(t)

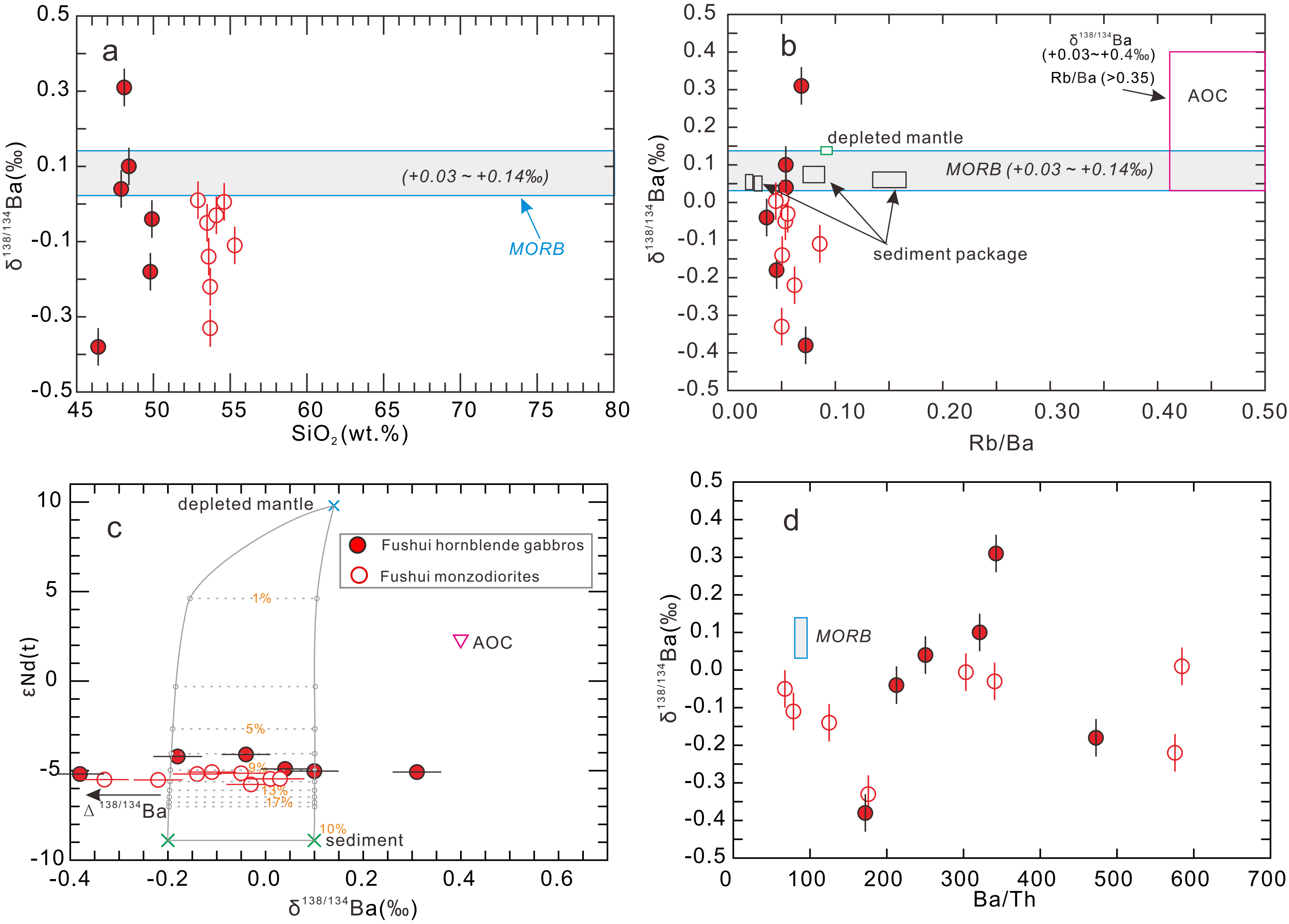
a
(+0.03 ~ +0.14‰)
MORB
$\delta^{138/134}$Ba(‰)
SiO_2(wt.%)
b
$\delta^{138/134}$Ba
(+0.03~+0.4‰)
Rb/Ba (>0.35)
AOC
depleted mantle
MORB (+0.03 ~ +0.14‰)
sediment package
$\delta^{138/134}$Ba(‰)
Rb/Ba
c
depleted mantle
Fushui hornblende gabbros
Fushui monzodiorites
AOC
1%
5%
9%
13%
17%
10%
sediment
$\Delta^{138/134}$Ba
εNd(t)
$\delta^{138/134}$Ba(‰)
d
MORB
$\delta^{138/134}$Ba(‰)
Ba/Th

Credit author statement

Lu-Lu Hao: Conceptualization, Methodology, Formal analysis, Investigation, Writing – original draft, Writing – review & editing. **Xiao-Yun Nan**: Conceptualization, Methodology, Formal analysis, Writing – original draft, Writing – review & editing. **Andrew C. Kerr**: Formal analysis, Investigation, Writing – original draft, Writing – review & editing. **Si-Qi Li**: Methodology, Formal analysis, Investigation, Writing – review & editing. **Yuan-Bao Wu**: Methodology, Formal analysis, Writing – review & editing. **Hao Wang**: Methodology, Formal analysis, Writing – review & editing. **Fang Huang:** Investigation, Writing – original draft, Writing – review & editing.

Declaration of interests

The authors declare that they have no known competing financial interests or personal relationships that could have appeared to influence the work reported in this paper.